The rapidly pulsating subdwarf B star PG1325+101. I. Oscillation modes from multisite observations

R. Silvotti, A. Bonanno, S. Bernabei, G. Fontaine, Stéphane Charpinet, S. Leccia, H. Kjeldsen, R. Janulis, A. Frasca, R. Ostensen, et al.

A&A 459, 557–564 (2006)
DOI: 10.1051/0004-6361:20065314

Astronomy & Astrophysics

The rapidly pulsating subdwarf B star PG 1325+101

I. Oscillation modes from multisite observations⋆,⋆⋆,⋆⋆⋆

R. Silvotti[1], A. Bonanno[2], S. Bernabei[3], G. Fontaine[4], S. Charpinet[5], S. Leccia[1], H. Kjeldsen[6], R. Janulis[7], A. Frasca[2], R. Østensen[8], S.-L. Kim[9], B.-G. Park[9], X. Jiang[10], M. D. Reed[11], R. S. Patterson[11], K. M. Gietzen[11], P. J. Clark[11], G. W. Wolf[11], Y. Lipkin[12], L. Formiggini[12], E. Leibowitz[12], T. D. Oswalt[13], M. Rudkin[13], K. Johnston[13], P. Brassard[4], P. Chayer[14,15], E. M. Green[16], and P. Bergeron[4]

(Affiliations can be found after the references)

Received 29 March 2006 / Accepted 11 May 2006

ABSTRACT

In this article we present the results of 215 h of time-series photometry on the rapidly pulsating subdwarf B star PG 1325+101 ($T_{\rm eff}$ = 35 000 K, $\log g = 5.8$, $\log N({\rm He})/N({\rm H}) = -1.7$), obtained during 25 days of observation in Spring 2003 from nine different sites. As in previous observations, the temporal spectrum is dominated by the main peak at 7255.55 μHz, with an amplitude of about 2.7% which, however, is dropped to about 1.7% in February 2005. No secondary peaks close to the dominant pulsation mode are clearly detected. In addition, at least fourteen more pulsation frequencies are found: three of them at 7704.92, 9380.17 and 14511.10 μHz were already present in the discovery run with small differences in frequency, probably due to 1-day aliasing effects. The peak at 7704.92 μHz belongs to a triplet of almost equally spaced frequencies that could be due to rotational splitting and would imply a rotational period of about 1.6 days. Based on the results of this article, a detailed asteroseismic analysis of PG 1325+101 is presented in a separate paper (Charpinet et al. 2006b, A&A, 459, 565, Paper II).

Key words. stars: horizontal-branch – stars: oscillations – stars: interiors – stars: individual: PG 1325+101

1. Introduction

Subluminous B (sdB) stars dominate the populations of faint blue stars of our own Galaxy and are found in both the disk (field sdBs) and the halo populations as blue tails to the horizontal branches of globular clusters (Ferraro et al. 1997). Observations with the Ultraviolet Imaging Telescope and the Hubble Space Telescope (Brown et al. 1997, 2000) have shown that these stars are sufficiently common to be the dominant source for the "UV upturn phenomenon" observed in elliptical galaxies and galaxy bulges (see also Dorman et al. 1995; Greggio & Renzini 1999). However, important questions remain over their exact evolutionary paths and appropriate time-scales.

It is now generally accepted that the sdB stars can be identified with Extreme Horizontal Branch (EHB) stars burning He in their core (Heber 1986; Saffer et al. 1994). Their inert hydrogen envelope is too thin (<1% by mass) to sustain nuclear burning and therefore, following stellar evolution calculations by Dorman et al. (1993), they are expected to bypass the Asymptotic Giant Branch and evolve directly to the white dwarf cooling track. Hence sdB stars can be considered as immediate progenitors of low mass white dwarfs but this evolutionary route is quite inefficient and only roughly 2% of the DA white dwarfs are formed from the sdB stars (Heber 1986). While the next stages of sdB evolution appear to be known, their prior evolution is still controversial. There have been three different scenarios proposed: i) binary interaction involving Roche lobe overflow (Mengel et al. 1976); ii) single star evolution with strong mass loss near the tip of the Red Giant Branch (D'Cruz et al. 1996); iii) merging of two helium white dwarfs (Iben & Tutukov 1986). Five different binary routes to form an sdB star (two based on common envelope ejection, two stable Roche lobe overflow models and the merger of two He WDs) have been systematically investigated by Han et al. (2003), using the radial velocity sample from Maxted et al. (2001) and Morales-Rueda et al. (2003) to calibrate their models. Lisker et al. (2005) compared the twelve simulation sets of Han et al. (2003) with a sample of 76 sdBs found in the SPY (=Supernovae type Ia Progenitor survey, Napiwotzki et al. 2003) project, the largest and most homogeneous sample obtained to date. They found that these simulation sets can reproduce well the observed distribution in $T_{\rm eff}$ and $\log g$, but not the slope of the observed cumulative luminosity function. The authors conclude that "a combination of single star and binary formation channels would be necessary to achieve full understanding of sdB formation processes". Another important element to compare observations with models is the fraction of radial velocity (RV) variables: Napiwotzki et al. (2004), using a subset of 46 stars from the SPY sample, found a frequency of 39% of RV variables, which increases up to 45% after correcting for the detection efficiency.

⋆ Based on observations obtained at the following telescopes: Loiano 1.5 m and Serra La Nave 0.9 m (Istituto Nazionale di Astrofisica), Moletai 1.65 m (Institute of Theoretical Physics and Astronomy, Vilnius), BOAO 1.8 m (Korea Astronomical Observatory), SARA 0.9 m (Southeastern Association for Research in Astronomy, Kitt Peak, Arizona), La Palma 0.6 m (KVA), BAO 0.85 m (Beijing Astronomical Observatory), Baker 0.4 m (Baker Observatory, Marshfield), Wise 1.0 m (Wise Observatory).

⋆⋆ Individual photometric measurements are only available in electronic form at the CDS via anonymous ftp to
`cdsarc.u-strasbg.fr (130.79.128.5)` or via
`http://cdsweb.u-strasbg.fr/cgi-bin/qcat?J/A+A/459/557`

⋆⋆⋆ Table 1 is only available in electronic form at
`http://www.aanda.org`

The discovery of multimode pulsators among the sdB stars has opened an attractive new possibility of probing their interiors using seismological methods. There are two classes of sdB pulsators (also called sdBV = sdB Variables) consisting firstly of 37 short-period variables (the last three discovered by Solheim & Østensen 2006), whose prototype is V361 Hya (or EC 14026, Kilkenny et al. 1997), that are characterized by short pulsation periods (∼1 to 10 min) caused by low-order acoustic waves (or *p*-modes). These oscillations are driven by an opacity bump associated with iron ionization (Charpinet et al. 1996). The second class was discovered more recently (Green et al. 2003) and consists of 25 pulsators having longer periods (∼30 min to 2 h), whose oscillations are associated with high-order gravity waves (or *g*-modes), analogous to our ocean waves. The driving mechanism for them could be again an opacity bump associated with iron ionization, but tidal forces in close binaries might be a possible alternative (Fontaine et al. 2003).

In both classes the iron enrichment in the driving layers below the atmosphere is caused by material being pushed up by radiative acceleration from deeper layers (Charpinet et al. 1997; Unglaub & Bues 2001). According to the predictions of microscopic elemental diffusion, the surface abundance of iron in sdB stars is mostly solar. However, a uniform solar metallicity would not drive pulsations in both types of pulsating sdB stars. Presently, there is no clear evidence of a significant overabundance of iron-group elements in pulsating sdBs with respect to the non-pulsating ones at similar effective temperatures. Recent results on a few sdBs from UV and far UV spectroscopy using HST/STIS (O'Toole et al. 2004) and FUSE (Chayer et al. 2004) are still contradictory.

The two sdBV instability strips have slightly different effective temperatures (∼28 000–36 000 K for the fast pulsators and ∼24 000–30 000 K for those with longer periods), with an overlap between about 28 000 and 30 000 K. The stars in this temperature range could in principle show both kinds of variability and indeed this is the case for at least two objects: HS 0702+6043 (Schuh et al. 2006) and Baloon 090100001 (Oreiro et al. 2004, 2005; Baran et al. 2005).

In this article we present a detailed study of the power spectrum of the sdB pulsator PG 1325+101 (hereafter PG 1325), that is located near the high gravity boundary of the short period sdBV instability strip. The variability of PG 1325 was discovered by Silvotti et al. (2002) in the framework of a search program at the Nordic Optical Telescope (Solheim et al. 2004) and further studied by Telting & Østensen (2004), who were able to see the radial-velocity and line-profile variations of the main pulsation mode. Based on the findings of the present paper, a detailed asteroseismic analysis of PG 1325 is presented in a separate paper by Charpinet et al. (2006b, hereafter Paper II). The asteroseismic solution described in Paper II is further improved using new higher quality determinations of the atmospheric parameters ($\log g = 5.81 \pm 0.04$, $T_{\rm eff} = 35\,050 \pm 220$ K and $\log N({\rm He})/N({\rm H}) = -1.70 \pm 0.02$, see Paper II for more details).

2. Observations and data reduction

PG 1325 was observed in Spring 2003, from March 21 to April 13, at nine different sites, resulting in 264 h of good data in 51 independent runs (see Table 1), which are reduced to 215 h considering the overlaps. Two kinds of different instruments were used: photoelectric photometers with B-peaked bialkali photomultipliers (PMTs) without any filter, as well as CCDs with standard B filters. The integration time was set to 10 s for all the PMTs and between 10 and 25 s for the CCDs, giving an effective sampling time between 12 and 30 s considering the read-out time. The light curve, shown in Fig. 1, is characterized by a duty cycle of 38%, which increases to 45% if we exclude the first short isolated run and the last one (which is quite noisy). Unfortunately, because of the "Pacific ocean gap", we were never able to reach 24 h of continuous coverage and therefore the 1-day aliases in the spectral window are still important (Fig. 3).

The data reduction was performed following standard procedures. For the PMT data, the sky was subtracted on a point-by-point basis when 3 channels were available. For the single channel photometer of Serra La Nave a linear interpolation was applied to the sky and comparison star measurements, which were done every 15–40 min, depending on the sky stability, and with a non-regular time sampling, in order to get a clean as possible spectral window. We then calculated the flux ratio between target and comparison star in order to compensate for the sky transparency variations. For the CCD data, bias and flat field corrections were applied; then aperture photometry was performed after subtracting the background. The flux ratios were obtained by dividing the counts of the target by the best combination of the available reference stars (between one and three). Finally, for both PMT and CCD data, the flux ratios of each run were converted to fractional intensities by dividing by the mean flux ratio of that run, and then to the so called milli-modulation intensity (mmi) units (1 mmi = 0.1% change in intensity) by subtracting unity and multiplying by 1000. The same definition applies to the milli-modulation amplitude (mma) units (1 mma = amplitude of 0.1%). Residual atmospheric extinction and further large time-scale variations, presumably due to sky transparency fluctuations, were then removed by means of a cubic spline interpolation. Intrinsic luminosity variations with periods of the order of 0.5 up to about 3 h were not observed, at least with amplitudes larger than a few percent. When data from more than one site were available at the same time, a weighted average was applied. As a final step, the times of the whole data set were converted to barycentric Julian date (BJD) using the algorithm of Stumpff (1980).

3. Data analysis

3.1. Statistical weights

The main problem of using large data sets from different sites, telescopes and instruments is that the quality of the data changes a lot from one observation to another. Taking this into account is important if we want to maximize the signal-to-noise (S/N) ratio in the power spectrum and detect as many pulsation frequencies as possible. One possible solution is to use a weighted Fourier transform (see e.g. Butler et al. 2004), where the statistical weights w_i are given by:

$$w_i = 1/\sigma_i^2. \quad (1)$$

Unfortunately, most of the data have no reported observational errors and therefore the first problem is to define the σ_i. Since the oscillation signal is the dominant cause of variations in the time series, as a first step we need to remove this signal from the data. This was done iteratively by finding the strongest peaks in the power spectrum and subtracting the corresponding sinusoids from the time series. At the end of this process we were left with a time series of residuals that reflects the noise properties of the measurements. For each of these residuals we then measured the standard deviation of the 100 points (or less when we are close

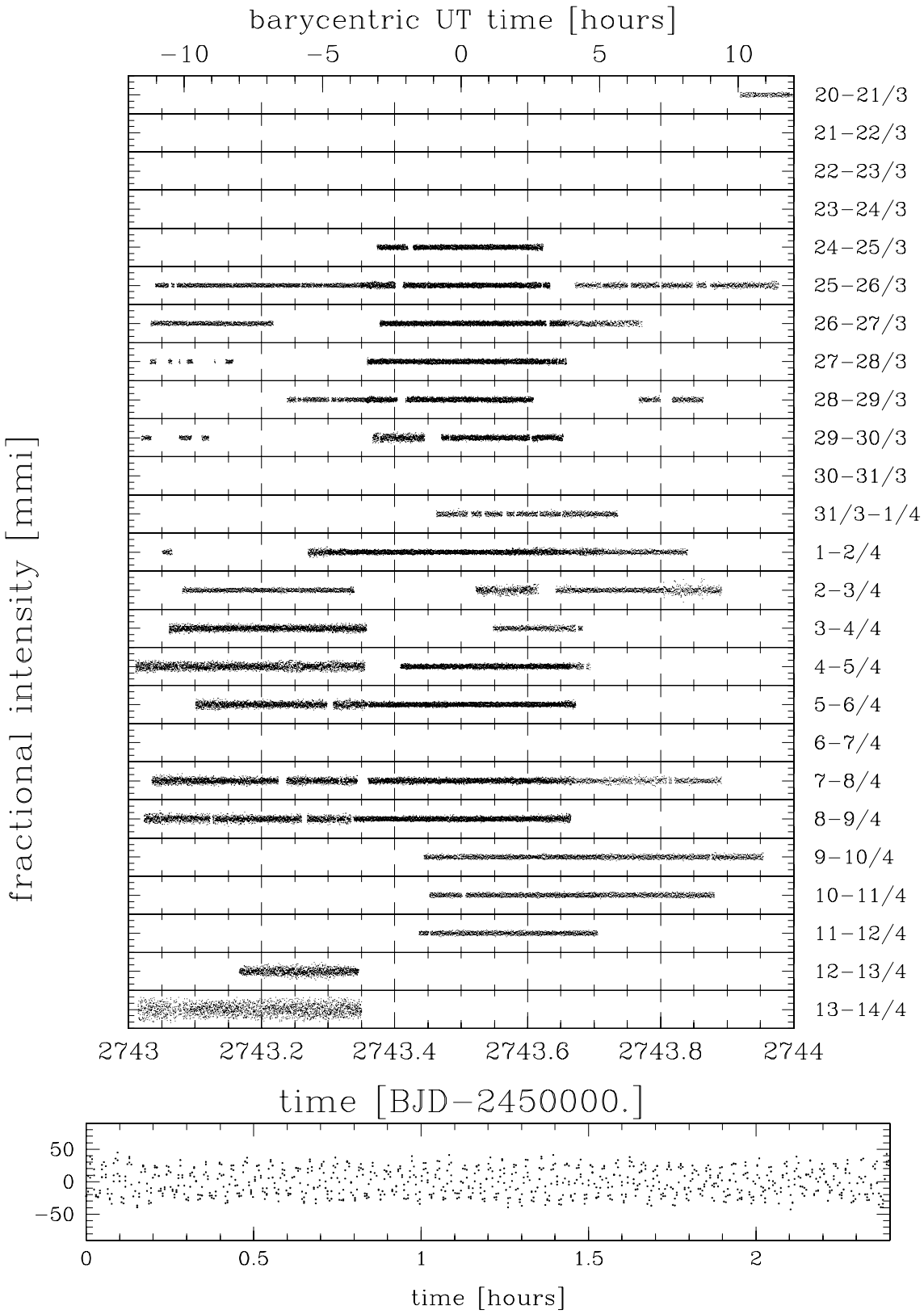

Fig. 1. The light curve of PG 1325+101 during the multisite run of March–April 2003. *Upper plot*: the whole data set. In this figure each panel represents 24 h and the vertical scale of each panel corresponds to 600 mmi (from –300 to 300), where mmi stands for milli-modulation intensity units (1 mmi = 0.1% variation). *Lower plot*: detail of the central part of the light curve from BJD 2731.45 to 2731.55 (April 1–2).

to the beginning or the end of a single data set) centered on it, and this was considered as the error σ_i of that measurement. In Fig. 2 the statistical weights obtained from this procedure are shown as a function of the scatter in the residuals series. Note that in this way we do not remove the bad data but simply give them a lower weight. The only exception was applied to the last

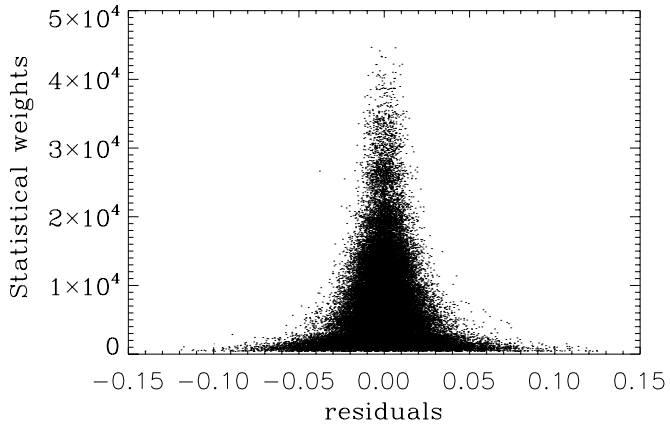

Fig. 2. Statistical weights as a function of the scatter in the residuals series (see the text for more details). Residuals are given as fractional intensities ($\Delta F/F$, where F is the measured flux). The non homogeneous distribution, with regions of higher density, is related to the different qualities of the observing runs.

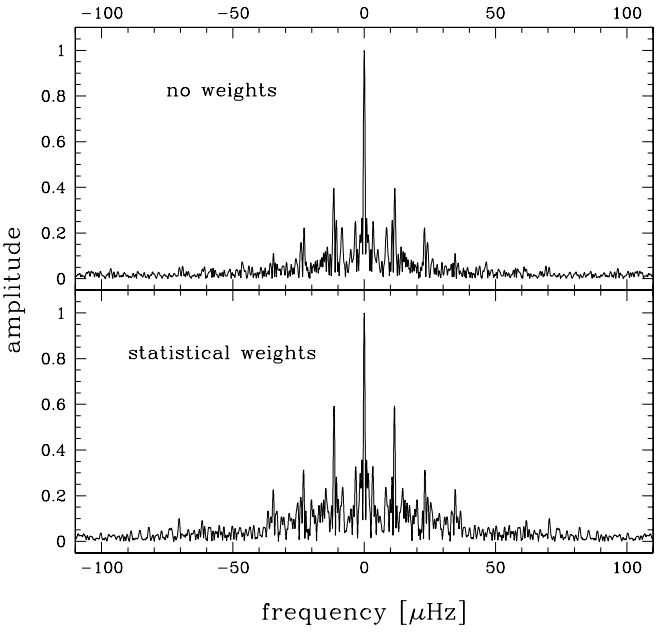

Fig. 3. Spectral window of the whole run with and without statistical weights. Note that the 1-day aliases increase from 40 to 59% when the weights are used. This is not surprising because using weights is equivalent to using less data in some parts of the overall light curve. Therefore the spectral window appears more noisy although the S/N ratio in the weighted Fourier transform is higher.

run of April 13, which was particularly noisy due to bad weather conditions, and that was simply removed from the data set used in our analysis.

The discrete Fourier transform (DFT) of the data, with and without statistical weights, is shown in Fig. 4. The average noise of the amplitude spectrum is decreased by a factor of about 1.5 when the weights are used. This allows us to identify one more peak at 5960.26 μHz and another two or three peaks around 10 000 μHz. On the other hand, in the region of maximum power near 7256 μHz, the noise of the weighted DFT is higher because of the degradation of the spectral window (Fig. 3).

3.2. Temporal stability of the amplitude spectrum

In order to check the stability of the spectrum over short time-scales, we divide the data set into three parts of similar length and calculate the DFT of each subset. As can be seen from the lower part of Fig. 4, the spectra are quite similar, suggesting a substantial stability over time-scales of the order of one week, although a few small amplitude peaks (at 6389.04, 10017.68 and 14511.10 μHz) show some possible variations. In any case, the amplitude of the main peak at 7255.55 μHz, which is not visible in the figure, is constant within the errors.

The same is not true over longer time-scales, of the order of years, as shown in Fig. 5, where the amplitude spectra at different epochs are compared. We clearly see that the peaks at ~7700 and 9380 μHz have significantly decreased their amplitude from July 2001 (discovery run, Silvotti et al. 2002) to March–April 2003. On the other hand, the main peak at 7255.55 μHz is constant within the errors (25.9 vs. 27.1 mma). However, this peak has lost significant power in the last run of February 2005, where its amplitude is reduced to 16.6 mma and where all the other peaks are below the noise level. Note that these differences can not be explained by the different efficiencies of the instruments used. The single site data of 2001 and 2005 were obtained with different telescopes (2.6 m NOT and 1.5 m Loiano respectively), but similar instruments (ALFOSC[1] and BFOSC[2]) and B filters. Regarding the multi-site data of 2003, the amplitude measurements can be partially affected by the different quantum efficiencies and transmission curves of the many instruments used (in particular between bialkali PMTs and CCDs), but these uncertainties can be estimated as being on the order of ~5% (see for instance the analysis of Kanaan et al. 2000, for pulsating white dwarfs). Indeed, a direct comparison between simultaneous PMT and CCD data on March 28 (Moletai vs BOAO) gave a difference of about 4% in amplitude.

3.3. Pre-whitening: extracting the pulsation frequencies

The pulsation frequencies were extracted by applying a pre-whitening technique: at each iteration the main frequency was subtracted from the data and the DFT of the residuals was recalculated, until the residuals were close to the noise level (Fig. 6). The results of this process, after having optimized frequencies, amplitudes and phases through a least-squares weighted sinusoidal fit, are reported in Table 2. However, to disentangle between real pulsation modes and artifacts is always a difficult task. Moreover, in the case of PG 1325 the spectrum is dominated by a single peak which has an amplitude at least 20 times higher than all the other signals. This makes it very difficult to extract possible weak signals close to the main peak. Therefore we divided Table 2 into two sections. The upper part reports the 15 best frequencies (named as $\boldsymbol{Fn}$, $n = 1, 15$), i.e. those which were directly visible in the original amplitude spectrum (before pre-whitening) and whose amplitude is equal to at least 4 times the local noise (defined as the average amplitude after pre-whitening in a region of typically ±100 μHz centered on the peak considered). The lower part of Table 2 reports another 15 frequencies which are more uncertain (named as $\boldsymbol{fn}$, $n = 1, 15$). Although many of these frequencies are probably due to artificial effects, we see from Fig. 6 (central panel) that the residual spectrum after having subtracted 15 frequencies still contains significant power;

[1] Andalucia Faint Object Spectrograph & Camera, see http://www.not.iac.es/instruments/alfosc/ for more details.

[2] Bologna Faint Object Spectrograph & Camera, see http://www.bo.astro.it/loiano/ for more details.

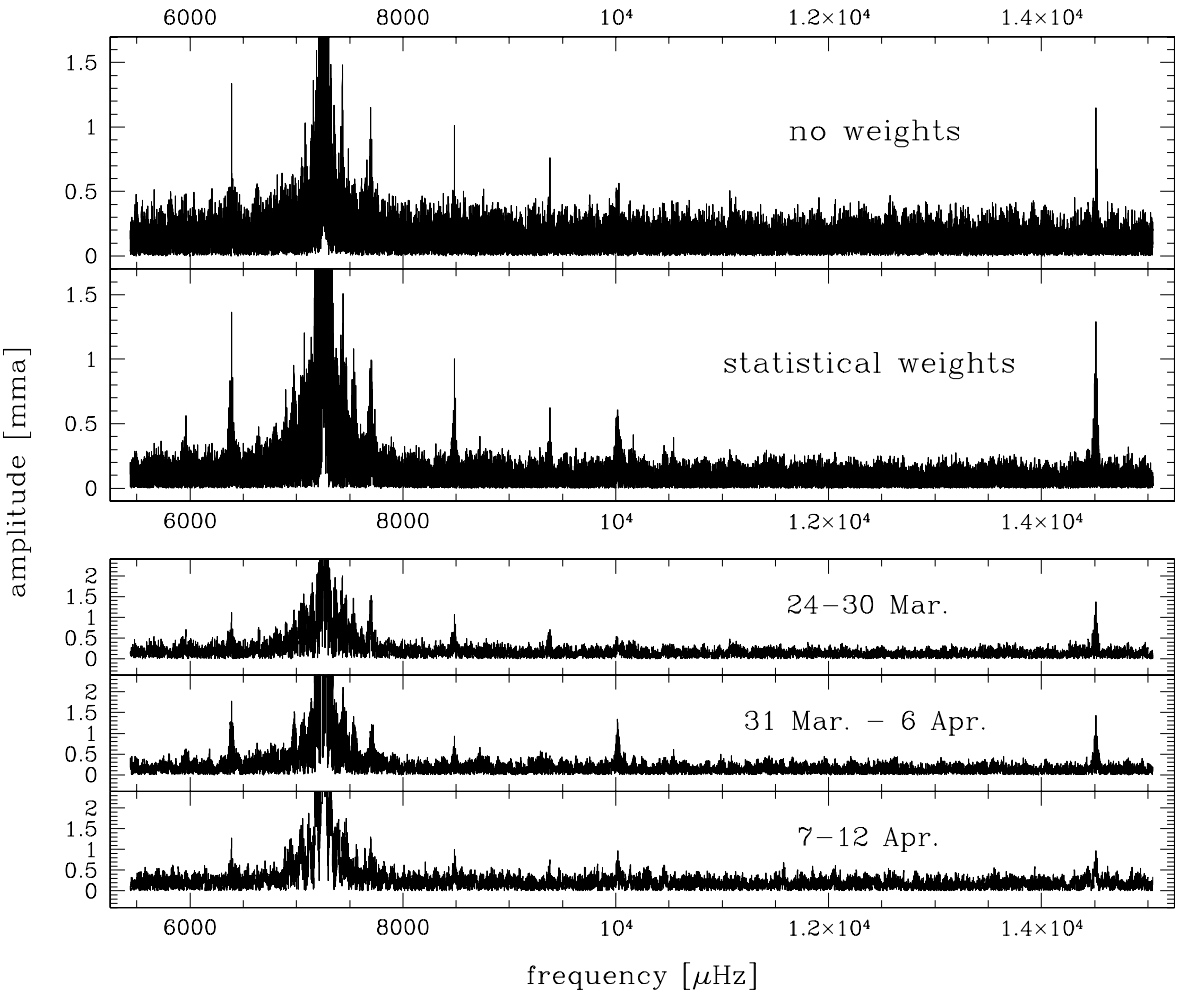

Fig. 4. Amplitude spectrum of PG 1325+101 with and without using weights. The three lower panels represent the weighted spectra of three subsets of data with similar length, each one covering almost one week. The amplitude is given in milli-modulation amplitude (mma) units, where 1 mma corresponds to an amplitude of 0.1%.

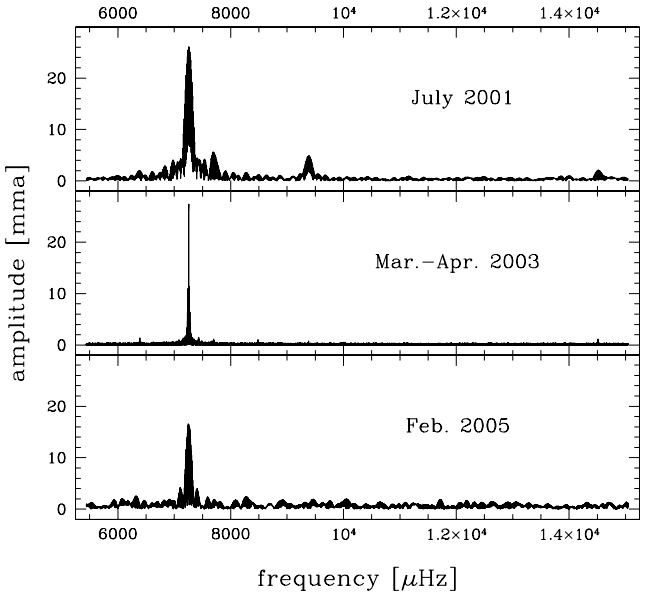

Fig. 5. Amplitude spectra of PG 1325+101 at different epochs: July 2001 (from Silvotti et al. 2002), March–April 2003 and February 2005. The latter was obtained from 5.3 h of CCD time-series data collected on February 12 and 14 (2005) at the Loiano 1.5 m telescope using the BFOSC camera + Johnson *B* filter.

therefore at least some of the peaks reported in the lower part of Table 2 must be due to true pulsation modes.

The uncertainties reported in Table 2 for amplitudes, frequencies and phases are the formal errors of the sinusoidal fit, based on the analytical estimates by Montgomery & O'Donoghue (1999):

$$\sigma(a) = \sqrt{\frac{2}{N}}\,\sigma(i) \;\simeq\; 0.10\ \mathrm{mma} \tag{2}$$

$$\sigma(f) = \sqrt{\frac{6}{N}}\,\frac{1}{\pi T}\,\frac{\sigma(i)}{a} = \frac{\sqrt{3}}{\pi T}\,\frac{\sigma(a)}{a} \;\simeq\; \frac{0.03}{a_{\mathrm{mma}}}\,\mu\mathrm{Hz} \tag{3}$$

$$\sigma(\phi) = \frac{1}{2\pi}\,\sqrt{\frac{2}{N}}\,\frac{\sigma(i)}{a} = \frac{1}{2\pi}\,\frac{\sigma(a)}{a} \;\simeq\; \frac{0.02}{a_{\mathrm{mma}}} \tag{4}$$

where $N = 56079$ is the number of data points, $T = 22.4$ the total duration of the run in days and $\sigma(i) = \langle\sigma_i\rangle = 0.01592$ is the mean error of the data (or mean error of the residual intensity as defined in Sect. 3.1). Note that $\sigma(a)$ represents the noise of the amplitude spectrum after pre-whitening and $\sigma(a)/a$ is the inverse of the S/N ratio. However, as pointed out by Montgomery & O'Donoghue (1999), the errors given by these formulae represent a lower limit to the real errors; in particular, the actual

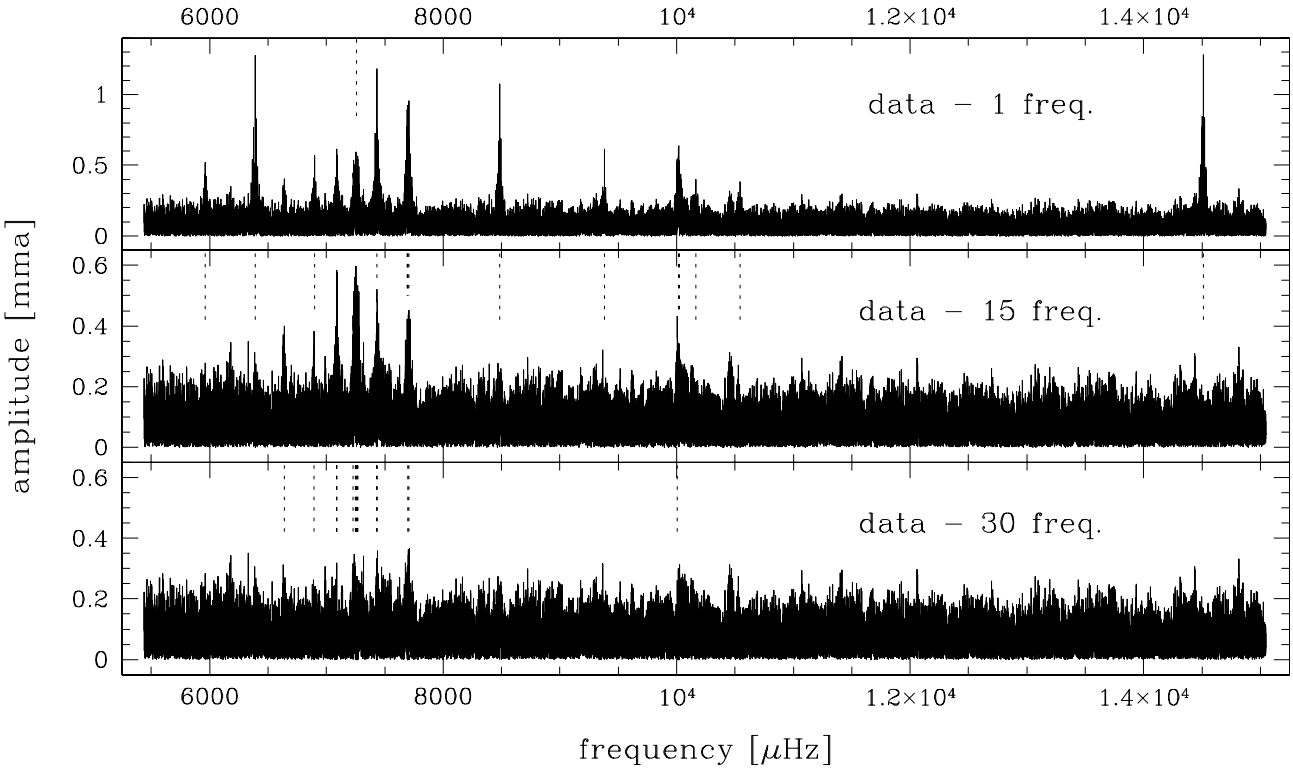

Fig. 6. The amplitude spectrum of PG 1325+101 at different steps of the pre-whitening procedure: starting from above, the spectrum is calculated after having subtracted the main signal (F4), the 15 best frequencies listed in the upper section of Table 2, 30 frequencies (upper + lower part of Table 2). The dotted lines represent the frequencies subtracted at each step.

Table 2. Results of the least-square sinusoidal fit (using weights) for the 15 best frequencies and 15 more suspected signals.

F [μHz][1]	P [s]	A [mma][1]	ϕ[1,2]	S/N[3]	Name
5960.258 ± 0.068	167.7780	0.53 ± 0.11	0.529 ± 0.031	5.5	F1
6389.037 ± 0.028	156.5181	1.29 ± 0.11	0.200 ± 0.013	12.8	F2
6897.344 ± 0.067	144.9834	0.54 ± 0.11	0.488 ± 0.030	5.7	F3
7255.549 ± 0.002	137.8256	27.12 ± 0.12	0.657 ± 0.001	239.3	F4
7431.097 ± 0.035	134.5696	1.12 ± 0.12	0.806 ± 0.016	10.9	F5
7691.036 ± 0.045	130.0215	0.82 ± 0.11	0.197 ± 0.021	7.5	F6
7698.664 ± 0.065	129.8927	1.04 ± 0.15	0.209 ± 0.030	8.1	F7
7704.918 ± 0.047	129.7872	0.97 ± 0.11	0.827 ± 0.021	9.3	F8
8484.680 ± 0.033	117.8595	1.08 ± 0.11	0.508 ± 0.015	12.4	F9
9380.169 ± 0.058	106.6079	0.61 ± 0.11	0.851 ± 0.026	6.5	F10
10017.680 ± 0.059	99.8235	0.65 ± 0.12	0.234 ± 0.026	6.0	F11
10019.204 ± 0.068	99.8083	0.61 ± 0.12	0.950 ± 0.030	4.5	F12
10164.744 ± 0.097	98.3793	0.37 ± 0.11	0.252 ± 0.044	4.0	F13
10545.219 ± 0.094	94.8297	0.38 ± 0.11	0.545 ± 0.042	4.0	F14
14511.096 ± 0.031	68.9128	1.28 ± 0.11	0.087 ± 0.013	14.7	F15 = 2F4
6639.427 ± 0.092	150.6154	0.39 ± 0.11	0.545 ± 0.041	4.2	f1
6891.787 ± 0.092	145.1002	0.39 ± 0.11	0.217 ± 0.041	4.1	f2
7087.283 ± 0.061	141.0978	0.60 ± 0.11	0.629 ± 0.027	6.4	f3
7089.645 ± 0.076	141.0508	0.48 ± 0.11	0.421 ± 0.034	4.9	f4
7228.214 ± 0.085	138.3468	0.44 ± 0.11	0.508 ± 0.038	3.8	f5
7247.132 ± 0.049	137.9856	0.84 ± 0.12	0.011 ± 0.021	4.7	f6
7252.547 ± 0.055	137.8826	0.71 ± 0.12	0.335 ± 0.025	5.2	f7
7259.310 ± 0.082	137.7541	0.51 ± 0.11	0.696 ± 0.034	4.4	f8
7266.034 ± 0.051	137.6267	0.77 ± 0.12	0.572 ± 0.024	4.8	f9
7269.114 ± 0.070	137.5683	0.56 ± 0.12	0.103 ± 0.031	4.0	f10
7430.157 ± 0.077	134.5867	0.49 ± 0.11	0.065 ± 0.035	3.8	f11
7434.945 ± 0.074	134.5000	0.51 ± 0.11	0.122 ± 0.033	4.4	f12
7698.230 ± 0.145	129.9000	0.46 ± 0.15	0.960 ± 0.065	3.8	f13
7704.319 ± 0.093	129.7973	0.50 ± 0.11	0.217 ± 0.041	4.3	f14
10007.298 ± 0.083	99.9271	0.49 ± 0.12	0.221 ± 0.038	3.9	f15

[1] The errors listed are the formal errors of the fit. [2] Phases in [0, 1] units are referred to the first datum at BJD = 2 452 719.919625. [3] *S/N* is defined as the ratio between amplitude and local average of the amplitude spectrum after pre-whitening.

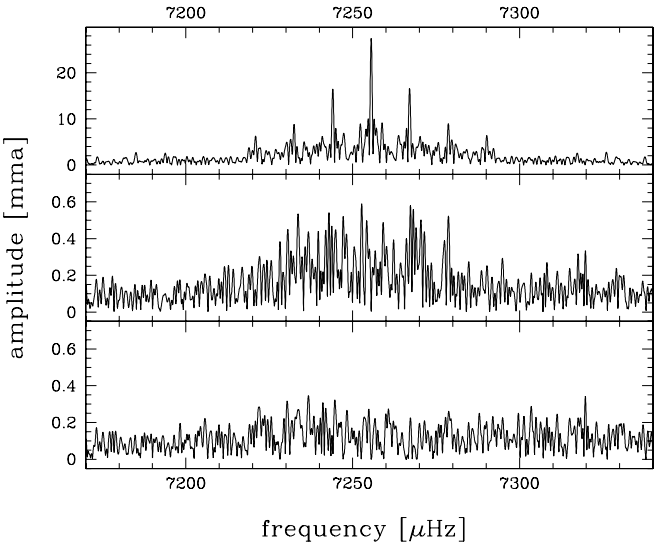

Fig. 7. Pre-whitening of the region near the main peak at 7255.55 μHz: the panels represent the amplitude spectrum before pre-whitening, after subtraction of the main peak (F4), and after subtraction of all the seven frequencies in the region near 7250 μHz (F4 plus f5 to f10, see Table 2). The huge difference in amplitude between the panels suggests that all the secondary peaks are not really significant. Further comments are given in the text.

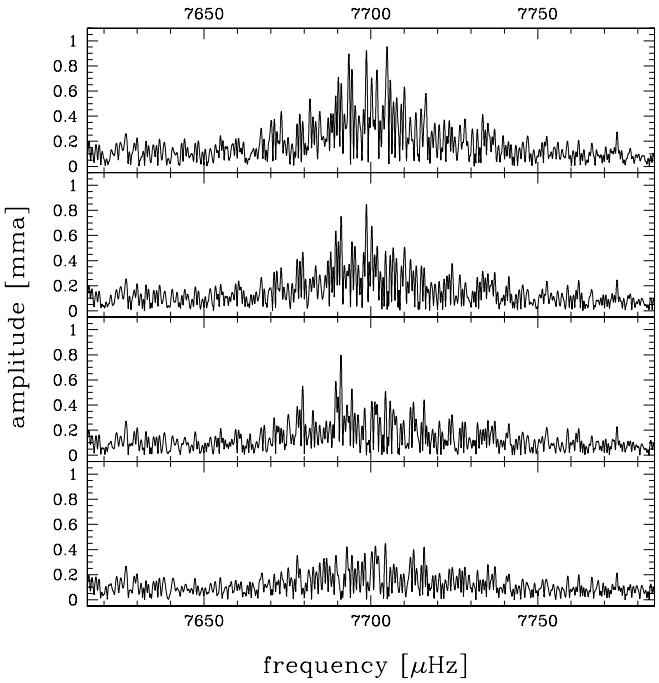

Fig. 8. Pre-whitening of the region near 7700 μHz where a triplet of almost equally spaced frequencies is found. Further comments are given in the text.

errors in frequency can be several times larger, up to a factor ≈10 (remembering that the formal resolution is only 0.52 μHz).

Considering the upper part of Table 2, we note that there are no peaks close to the main signal at 7255.55 μHz. All six frequencies obtained from the pre-whitening in the range 7228.21–7269.11 μHz, reported in the lower section of Table 2, have relatively low S/N ratios and could easily be the product of some artificial effect during the subtraction of the various sinusoids. A detail of the pre-whitening applied to this region is given in Fig. 7. Therefore we conclude that there is no clear evidence of secondary peaks in the region near the main peak at 7255.55 μHz. This result apparently supports the suggestion of Telting & Østensen (2004) that the main peak, with an RV amplitude of 18 km s^{-1}, could be an $l = 0$ mode. However, the detailed asteroseismic analysis reported in Paper II leads to a different conclusion and points towards an $l = 2$ mode.

Another interesting point concerns the peak at 7698.66 μHz, which in 2001 was observed at about 7713 μHz, a difference of ∼14.3 μHz. Considering that the uncertainty in frequency of that run was of the order of 2.7 μHz, it is likely that the peak detected in 2001 was simply the 1-day alias of the true value, that falls at 7710.23 (7698.66+11.57) μHz. The same argument applies to the high frequency peak at 14511.10 μHz, which in 2001 was found at 14523 μHz: the difference is very close to 11.57 μHz. Note that the new and much more precise value corresponds exactly to the first harmonic of the main peak ($7255.55 \times 2 = 14511.10$).

Finally, looking at Table 2, we note two groups of close frequencies near 7700 and 10 000 μHz. In particular, the first group, which is highlighted in Fig. 8, is formed by a triplet of almost equally spaced frequencies at 7691.04, 7698.66 and 7704.92 μHz. Their spacings are equal to 7.62 and 6.26 μHz, with an average value of 6.94 μHz. If this effect was due to rotational splitting and considering a spherical harmonic index $l = 1$, the rotational period of the star $P_{\rm rot} = (1–C_{nl})/\Delta f$ would be equal to about 1.6 days (considering a value smaller than 0.07 for the constant C_{nl} related to the stellar structure). Indeed, looking at Paper II, we see that the best-fit model points towards $l = 1$ for the triplet and therefore, using the best value $C_{31} = 0.014$, we obtain $P_{\rm rot} = 1.6 \pm 0.2$ days (i.e. $V_{\rm eq}$ on the order of 5 km s^{-1}). Unfortunately this result can not be directly verified by the spectroscopy: the time resolved spectra of Telting & Østensen (2004) have a resolution of the order of $R = 500$, not sufficient to detect such low RV variations. Moreover a low RV variation is hard to see due to the pulsational line broadening. However, from the higher resolution MMT spectrum reported in Paper II we can at least derive an upper limit to the projected rotational velocity of the order of 20–30 km s^{-1} (see Paper II for more details).

4. Summary

The analysis of our multisite time-series observations on PG 1325 shows that this star has a rich frequency spectrum, with at least 15 pulsation frequencies in the range between 5960 and 10545 μHz ($94.8 < P < 167.8$ s). The spectrum is dominated by a strong peak at 7255.55 μHz (137.8 s) with an amplitude of 27.1 mma, whereas all the other frequencies have much lower amplitudes, below 1.3 mma. The first harmonic of the main peak is also detected, with a period of only 68.9 s. The spectrum appears rather stable over short time-scales (no variations are seen during our ∼3 weeks run) but shows significant variations over longer time-scales (years). Because of its rich frequency spectrum and relative brightness, PG 1325 is a good target for seismological studies together with a few other rapid sdB pulsators like PG 1605+072, PB 8783, PG 0014+067, PG 1047+003, PG 1219+534, Feige 48 and Baloon 090100001, some of them having already been studied in great detail (O'Donoghue et al. 1998; Kilkenny et al. 1999; Reed et al. 2004; Charpinet et al. 2006a; Vučković et al. 2006; Baran et al. 2006). Indeed, the seismic analysis reported in paper II demonstrates that a good solution can be obtained, matching all twelve independent

frequencies, and in excellent agreement with the atmospheric parameters obtained from spectroscopy. Moreover, a triplet of close frequencies is detected, centered around 7698.66 μHz. Considering a value $l = 1$ (and $k = 3$), as indicated by the best model fit of Paper II, this triplet suggests a low rotation velocity with a period $P_{\rm rot} = 1.6 \pm 0.2$ days.

Acknowledgements. Part of this work was supported by the Italian research foundation MIUR under project "COFIN Astrosismologia" (coordinator L. Paternò). R.S. is grateful to the Catania asteroseismology group for the kind hospitality during his short stay in April 2005, in which part of this work was done. The SARA observations were supported by NSF grant AST-0206115. Our analysis has made use of the software Period04 (Lenz & Breger 2005). The authors wish to thank David Kilkenny for many usefull suggestions given in the referee report, and Chris Heines for having contributed to improve the english.

References

Baran, A., Pigulski, A., Koziel, D., et al. 2005, MNRAS, 360, 737
Baran, A., Oreiro, R., Pigulski, A., Pérez Hernández, F., & Ulla, A. 2006, Baltic Astron., 15, 227
Brassard, P., Fontaine, G., Billères, M., et al. 2001, ApJ, 563, 1013
Brown, T. M., Ferguson, H. C., Davidsen, A. F., & Dorman, B. 1997, ApJ, 482, 685
Brown, T. M., Bowers, C. W., Kimble, R. A., Sweigart, A. V., & Ferguson, H. C. 2000, ApJ 532, 308
Butler, R. P., Bedding, T. R., Kjeldsen, H., et al. 2004, ApJ, 600, L75
Charpinet, S., Fontaine, G., Brassard, P., & Dorman, B. 1996, ApJ, 471, L106
Charpinet, S., Fontaine, G., Brassard, P., et al. 1997, ApJ, 483, L123
Charpinet, S., Fontaine, G., Brassard, P., Chayer, P., & Green, E. M. 2006a, Baltic Astron., 15, 305
Charpinet, S., Silvotti, R., Bonanno, A., et al. 2006b, A&A, 459, 565 (Paper II)
Chayer, P., Fontaine, G., Fontaine, M., et al. 2004, Ap&SS, 291, 359
D'Cruz, N. L., Dorman, B., Rood, R. T., & O'Connell, R. W. 1996, ApJ, 466, 359
Dorman, B., O'Connell, R. W., & Rood, R. T. 1993, ApJ, 419, 596
Dorman, B., O'Connell, R. W., & Rood, R. T. 1995, ApJ, 442, 105
Ferraro, F. R., Paltrinieri, B., Fusi Pecci, F., et al. 1997, ApJ, 484, L145
Green, E. M., Fontaine, G., Reed, M. D., et al. 2003, ApJ, 583, L31
Fontaine, G., Brassard, P., Charpinet, S., et al. 2003, ApJ, 597, 518
Greggio, L., & Renzini, A. 1999, Mem. S. A. It., 70, 691
Han, Z., Podsiadlowski, Ph., Maxted, P. F. L., & Marsh, T. R. 2003, MNRAS, 341, 669
Heber, U. 1986, A&A, 155, 33
Iben, I. J., & Tutukov, A. V. 1986, ApJ, 311, 753
Kanaan, A., O'Donoghue, D., Kleinman, S. J., et al. 2000, Baltic Astron., 9, 387
Kilkenny, D., Koen, C., O'Donoghue, D., & Stobie, R. S. 1997, MNRAS, 285, 640
Kilkenny, D., Koen C., O'Donoghue, D., et al. 1999, MNRAS, 303, 525
Lenz, P., & Breger, M., 2005, Commun. Asteroseismol., 146, 53
Lisker, T., Heber, U., Napiwotzki, R., et al. 2005, A&A, 430, 223
Maxted, P. F. L., Heber, U., Marsh, T. R., & North, R. C. 2001, MNRAS, 326, 1391
Mengel, J. G., Norris, J., & Gross, P. G. 1976, ApJ, 204, 488
Montgomery, M. H., & O'Donoghue, D. 1999, Delta Scuti Stars Newsletter, 13
Morales-Rueda, L., Maxted, P. F. L., Marsh, T. R., North, R. C., & Heber, U. 2003, MNRAS, 338, 752
Napiwotzki, R., Christlieb, N., Drechsel, H., et al. 2003, ESO Messenger, 112, 25
Napiwotzki, R., Karl, C. A., Lisker, T., et al. 2004, Ap&SS, 291, 321
O'Donoghue, D., Koen, C., Solheim, J.-E., et al. 1998, MNRAS, 296, 296
Oreiro, R., Ulla, A., Pérez Hernández, F., et al. 2004, A&A, 418, 243
Oreiro, R., Pérez Hernández, F., Ulla, A., et al. 2005, A&A, 438, 257
O'Toole, S. J., Heber, U., Chayer, P., et al. 2004, Ap&SS, 291, 427
Reed, M. D., Kawaler, S. D., Zola, S., et al. 2004, MNRAS, 348, 1164
Saffer, R. A., Bergeron, P., Koester, D., & Liebert, J. 1994, ApJ, 432, 351
Schuh, S., Huber, J., Dreizler, S., et al. 2006, A&A, 445, L31
Silvotti, R., Østensen, R., Heber, U., et al. 2002, A&A, 383, 239
Solheim, J.-E., Østensen, R., Silvotti, R., & Heber, U. 2004, Ap&SS, 291, 419
Solheim, J.-E., & Østensen, R. 2006, Baltic Astron., 15, 231
Stumpff, P. 1980, A&AS, 41, 1
Unglaub, K., & Bues, I. 2001, A&A, 374, 570
Telting, J. H., & Østensen, R. H. 2004, A&A, 419, 685
Vučković, M., Kawaler, S. D., O'Toole, S., et al. 2006, ApJ, submitted

[1] INAF - Osservatorio Astronomico di Capodimonte, via Moiariello 16, 80131 Napoli, Italy
e-mail: [silvotti;leccia]@na.astro.it
[2] INAF - Osservatorio Astrofisico di Catania, via S. Sofia 78, 95123 Catania, Italy
e-mail: [alfio;afr]@ct.astro.it
[3] INAF - Osservatorio Astronomico di Bologna, via Ranzani 1, 40127 Bologna, Italy
e-mail: bernabei@bo.astro.it
[4] Département de Physique, Université de Montréal, CP 6128, Succursale Centre-Ville, Montréal, QC, H3C3J7, Canada
e-mail: [fontaine;bergeron;brassard]@astro.umontreal.ca
[5] UMR 5572, Université Paul Sabatier et CNRS, Observatoire Midi-Pyrénées, 14 Av. E. Belin, 31400 Toulouse, France
e-mail: scharpin@ast.obs-mip.fr
[6] Institut for Fysik og Astronomi (IFA), Aarhus Universitet, 8000 Aarhus, Denmark
e-mail: hans@phys.au.dk
[7] Institute of Theoretical Physics and Astronomy, Vilnius University, Lithuania
e-mail: jr@itpa.lt
[8] Isaac Newton Group, S. Cruz de La Palma, Canary Islands, Spain
[9] Korea Astronomy and Space Science Institute, South Korea
e-mail: [slkim;bgpark]@kasi.re.kr
[10] National Astronomical Observatories, Beijing, 100012, PR China
e-mail: xjjiang@bao.ac.cn
[11] Missouri State University and Baker Observatory, 901 S. National, Springfield, MO 65897, USA
e-mail: [mikereed;rsp814f;gww836f]@missouristate.edu
[12] Wise Observatory, Israel
e-mail: [yiftah;lili;elia]@wise.tau.ac.il
[13] Department of Physics and Space Sciences and the SARA Observatory, Florida Institute of Technology, 150 West University Boulevard, Melbourne, FL 32901, USA
e-mail: [toswalt;mrudkin;kyjohnst]@fit.edu
[14] Department of Physics and Astronomy, Johns-Hopkins University, 3400 North Charles St., Baltimore, MD 21218-2686, USA
e-mail: chayer@pha.jhu.edu
[15] Department of Physics and Astronomy, University of Victoria, PO Box 3055, Victoria, BC V8W 3P6, Canada
[16] Steward Observatory, University of Arizona, 933 North Cherry Av., Tucson, AZ 85721, USA
e-mail: bgreen@as.arizona.edu

Online Material

Table 1. Observing log.

$Date_{start}$	UT_{start}	Duration [h]	Telescope	Instr.	Observers
21/03/03	09:56:41.0	1.8	SARA 0.9 m	CCD	TDO, MR
24/03/03	20:50:45.0	5.8	Moletai 1.65 m	3ch.PMT	RJ
25/03/03	12:50:27.0	7.1	BOAO 1.8 m	CCD	SLK, BGP
25/03/03	20:15:45.0	5.3	Moletai 1.65 m	3ch.PMT	RJ
25/03/03	21:47:05.9	3.3	Serra la Nave 0.9 m	1ch.PMT	AB, AF
26/03/03	03:59:03.5	6.8	Baker 0.4 m	CCD	MDR
26/03/03	12:40:47.0	4.4	BOAO 1.8 m	CCD	SLK, BGP
26/03/03	20:56:20.2	6.0	Serra la Nave 0.9 m	1ch.PMT	AB, AF
26/03/03	21:01:45.0	5.9	Moletai 1.65 m	3ch.PMT	RJ
27/03/03	03:33:04.0	2.8	Baker 0.4 m	CCD	MDR
27/03/03	12:39:17.0	0.9	BOAO 1.8 m	CCD	SLK, BGP
27/03/03	20:28:00.5	6.2	Serra la Nave 0.9 m	1ch.PMT	AB, AF
27/03/03	20:41:45.0	5.8	Moletai 1.65 m	3ch.PMT	RJ
28/03/03	17:35:52.0	2.5	BOAO 1.8 m	CCD	SLK, BGP
28/03/03	19:55:15.0	6.3	Moletai 1.65 m	3ch.PMT	RJ
29/03/03	06:18:56.2	1.9	Baker 0.4 m	CCD	MDR, PJC
29/03/03	12:20:17.0	1.1	BOAO 1.8 m	CCD	SLK, BGP
29/03/03	20:40:55.0	4.1	Moletai 1.65 m	3ch.PMT	RJ
29/03/03	23:09:33.2	4.2	Serra la Nave 0.9 m	1ch.PMT	AB, AF
30/03/03	12:17:47.0	3.2	BOAO 1.8 m	CCD	SLK, BGP
31/03/03	22:58:31.6	5.9	La Palma 0.6 m	CCD	RØ
01/04/03	13:05:27.0	0.4	BOAO 1.8 m	CCD	SLK, BGP
01/04/03	18:20:52.6	4.0	Wise 1.0 m	CCD	YL, LF, EL
01/04/03	19:03:15.0	6.6	Moletai 1.65 m	3ch.PMT	RJ
01/04/03	20:56:35.0	6.1	Loiano 1.5 m	3ch.PMT	RS, SB
02/04/03	00:32:22.6	3.8	La Palma 0.6 m	CCD	RØ
02/04/03	03:07:33.0	4.8	Baker 0.4 m	CCD	MDR, KMG
02/04/03	13:48:37.0	6.0	BOAO 1.8 m	CCD	SLK, BGP
02/04/03	18:17:16.6	3.9	Wise 1.0 m	CCD	YL, LF, EL
03/04/03	03:19:11.0	6.0	Baker 0.4 m	CCD	RSP, PJC
03/04/03	13:19:55.0	7.1	BAO 0.85 m	3ch.PMT	XJ
04/04/03	01:01:30.9	3.1	La Palma 0.6 m	CCD	RØ
04/04/03	01:35:16.6	1.1	Wise 1.0 m	CCD	YL, LF, EL
04/04/03	12:07:15.0	8.3	BAO 0.85 m	3ch.PMT	XJ
04/04/03	21:41:25.0	6.3	Loiano 1.5 m	3ch.PMT	RS, SB
04/04/03	22:39:25.9	5.7	La Palma 0.6 m	CCD	RØ
05/04/03	14:17:05.0	5.9	BAO 0.85 m	3ch.PMT	XJ
05/04/03	19:52:40.7	6.7	Serra la Nave 0.9 m	1ch.PMT	AB, AF
05/04/03	20:38:16.0	7.4	Loiano 1.5 m	3ch.PMT	RS, SB
07/04/03	12:43:05.0	7.1	BAO 0.85 m	3ch.PMT	XJ
07/04/03	20:29:45.0	7.4	Loiano 1.5 m	3ch.PMT	RS, SB
08/04/03	03:10:50.3	5.8	Baker 0.4 m	CCD	MDR, PJC
08/04/03	12:25:45.0	7.1	BAO 0.85 m	3ch.PMT	XJ
08/04/03	19:57:55.0	7.9	Loiano 1.5 m	3ch.PMT	RS, SB
09/04/03	22:32:03.9	6.4	La Palma 0.6 m	CCD	RØ
10/04/03	03:21:21.0	7.4	Baker 0.4 m	CCD	RSP, PJC
10/04/03	22:44:10.9	6.0	La Palma 0.6 m	CCD	RØ
11/04/03	03:16:04.1	5.6	Baker 0.4 m	CCD	MDR, KMG
11/04/03	22:21:02.9	6.4	La Palma 0.6 m	CCD	RØ
12/04/03	15:51:45.0	4.3	BAO 0.85 m	3ch.PMT	XJ
13/04/03	12:13:05.0	7.9	BAO 0.85 m	3ch.PMT	XJ